Study on Surface Depression of Ti-6Al-4V with Ultrahigh-Frequency Pulsed Gas Tungsten Arc Welding

YANG MINGXUAN, YANG ZHOU, and QI BOJIN

Molten pool surface depression was observed with the arc welding process that was caused by arc pressure. It was supposed to have a significant effect on fluid in the molten pool that was important for the microstructure and joint properties. The impact of arc force was recognized as the reason for the surface depression during arc welding. The mathematical distribution of arc force was produced with the exponent and parabola models. Different models showed different concentrations and attenuations. The comparison between them was discussed with the simulation results. The volume of fluid method was picked up with the arc force distribution model. The surface depression was caused by the arc force. The geometry of the surface depression was discussed with liquid metal properties. The welding process was carried out with different pulsed frequencies. The results indicated the forced depression exists in molten pool and the geometry of depression was hugely due to the arc force distribution. The previous work calculated the depression in the center with force balance at one point. The other area of gas shielding was resistant by the reverse gravity from the feedback of liquid metal that was squeezed out. The article discusses the pressure effect with free deformation that allowed resistance of liquid and was easy to compare with different distributions. The curve profiles were studied with the arc force distributions, and exponent model was supposed to be more accurate to the as-weld condition.

DOI: 10.1007/s11663-015-0381-3

I. INTRODUCTION

ARC welding is a traditional process technology in industry. Surface depression can be observed with the arc welding process.[1–3] It was caused by an impact of arc plasma or arc pressure. Lin and Eagar indicated that the surface depression was created by arc pressure that caused forced vortex,[4] and significant penetration can be found with large pressure.[5,6] Jia and Cook demonstrated that the arc force varied with square welding current and the plasma jet force was the crucial element of arc force.[7,8] With less than 200 A, the plasma drag force can be ignored as a driving force of molten pool in previous research[9]; however, it was still an important factor for the surface depression. The force model was improved by Rokhlin and Guu, who discussed the correlation between the arc force and the surface depression during arc welding.[10] The force balance of surface tension, liquid pressure, and arc force was the key source for the analysis. In the previous research with pulsed arc welding, the large arc force was created with high-frequency pulsed current.[11,12] The effect of arc force on surface deformation was described by modeling with stainless steel,[13] and deep depression was predicted with titanium alloys. The results indicated the huge effect of surface depression on the fluid in molten pool, including melting process, temperature distribution, and liquid velocity, which were important for fluidity and solidification.

The fluid status and welds can be recognized as the presentation of dynamic physical phenomenon of arc plasma. Conventional thermal cycle with arc welding caused overheating to the base metal, which is recognized as the reason for the obvious grain growth,[14,15] and the fluid of molten pool had effect on subsequent heat transfer and solidification of welds.[16] Some research results have demonstrated the effect of pulsed arc welding on weld appearance,[17] microstructure morphology, and mechanical properties.[18] Grain refinement,[19] toughness, and optimized ductility[20,21] were found with titanium alloys from 6 to 80 kHz. Above all, surface depression in molten pool represents the characteristics of arc welding that can affect the fluid status and heat-transfer process. It is the dominance of microstructure and joints' properties, which is meaningful for welds. A previous study referred to the arc force and molten pool during conventional gas tungsten arc welding (C-GTAW) and ultrahigh-frequency pulsed gas tungsten arc welding (UHFP-GTAW). The arc force was measured and an increasing trend can be found with UHFP-AW. For the molten pool, the mathematical model was established for surface depression calculation, which was important to study fluid in the molten pool.[22] In that work, the surface depression was

YANG MINGXUAN, Lecturer, YANG ZHOU, Ph.D. Candidate, and QI BOJIN, Professor, are with the Department of Materials Processing, Beijing University of Aeronautics and Astronautics, Beijing 10000, P.R. China. Contact e-mail: yangmingxuan@buaa.edu.cn
Manuscript submitted February 11, 2015.
Article published online June 12, 2015.

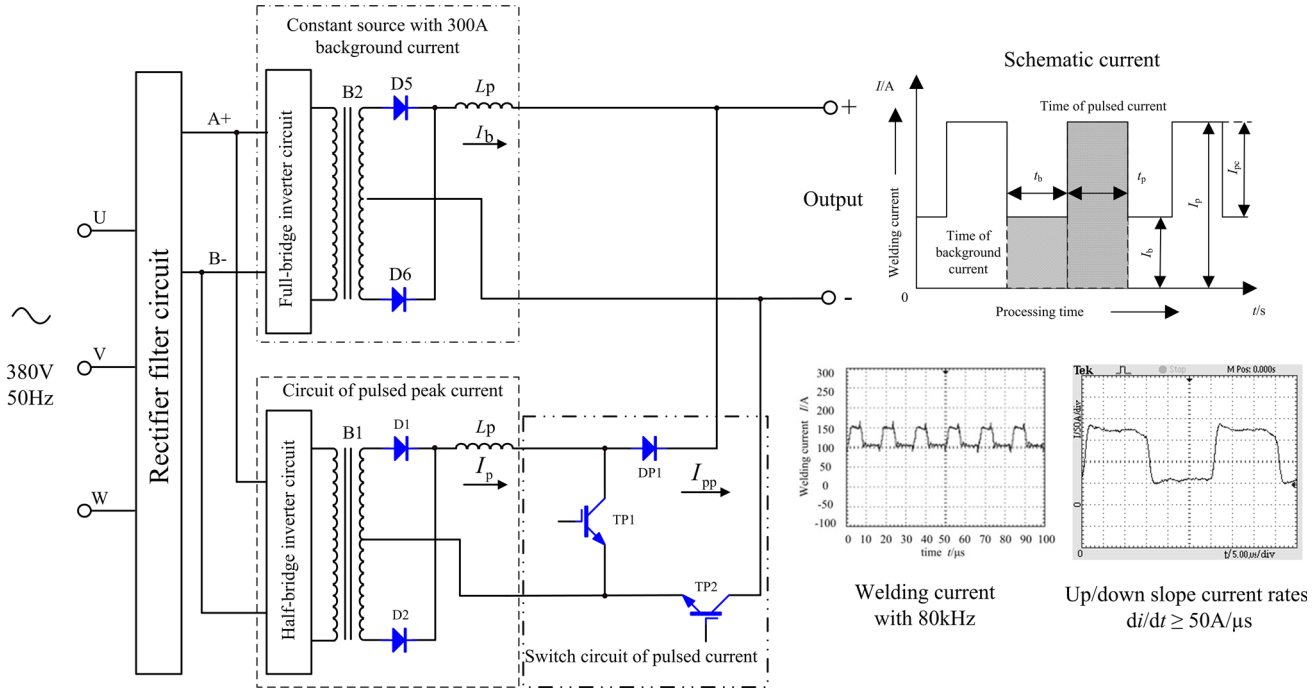

Fig. 1—Welding current with UHFP-GTAW.

assumed to be an arc profile, and an ellipsoid was used with 80 kHz as it was out of the original assumption. However, in that work, all the surface depressions were predicted with the preset regular shape, which was due to the calculation process. The resistance against arc pressure was only liquid pressure and gravity. Thus, the geometry of surface depression was not discussed with free deformation. The resistance of fluid was ignored during previous work. Actually, such a depression on the fluid surface was created by external pressure as introduced before. It is believed that there will be some correlation between the geometry and the distribution of the pressure. With classic physics, some physical quantities follow a similar Gaussian distribution. The exponent model stands for the most distribution with a high concentration and large attenuation that is similar to the Gaussian function. The parabola model has opposite characteristics. Furthermore, the free deformation with external pressure will allow the effect of resistance of squeezed liquid metal, which is more accurate and closer to reality.

As described before, the surface depression created by arc pressure was meaningful for microstructure and joint properties. The study focused on the effect of arc pressure on surface of the molten pool. Different welding methods were produced with conventional arc welding (C-GTAW) and ultrahigh-frequency pulsed arc welding (UHFP-GTAW). Various mathematical functions of arc force distribution were carried out with the exponent and parabola model. The comparison was discussed with the simulation results of surface depression that was made by the arc forces following the volume of fluid (VOF) model.

II. METHODS

A. *Stationary Welding Experiments*

The material studied was Ti-6Al-4V alloy (thickness $h_t = 2$ mm). C-GTAW was set as a contrast experimental group. UHFP-GTAW was carried out with the current upslope/downslope rate (di/dt) equal to 50 A/μs, which was achieved with an insulated gate bipolar transistor switch component. A schematic diagram of the weld current is illustrated in Figure 1. Full and half-bridge invert circuits are used. The switch component has a high withstand voltage and can resistant more than 500 V, which secured the high frequency and large converting speed di/dt. With previous work (Reference 13), the arc force can be obtained with the measurement apparatus. The parameters were shown in Table I, in which No. *s-i* is stainless steel and No. *t-j* is a titanium alloy.whereas I_b/I_p was background/pulsed current and f is the pulse frequency. Time of background and pulsed currents were t_b and t_p, respectively, and the duty cycle of pulse duration can be deduced as $\delta = t_p / (t_b + t_p)$.

The scale of the workpiece is 30 × 10 × 2 mm^3 (titanium alloy) for the arc force measurements. The conventional parameters were as follows: The electrode radius was 1.2 mm and made of 2 pct cerium and 98 pct tungsten, the arc length was 3 mm, and the gas was 99.99 pct argon. The base metal was stored in a dry cleaning utensil before welding. During arc force measurement, with a spot weld, each group will hold the stationary arc plasma for more than 5 seconds, and the data will be transported from the sensor to acquisition card.

Table I. Parameters of Welding Process

No.	I_b/A	I_p/A	f/kHz	δ (pct)	Argon q_c /(L min^{-1})
t-1	80	—	—	—	15
t-2	40	100	20	50	15
t-3	40	100	40	50	15
t-4	40	100	60	50	15

Table II. Physical Properties of Ti-6Al-4V

Physical Properties	Value
Liquidus temperature, T_l (K)	1928[23]
Solidus temperature, T_s (K)	1878[23]
Liquid density, ρ (kg/m^3)	4450
Liquid viscosity, μ (kg/ms)	0.0049
Solid phase effective thermal conductivity, k_s (J/ms K)	5.4
Liquid phase effective thermal conductivity, k_l (J/ms K)	15.9
Solid phase specific heat capacity, C_{PS} (J/kg K)	879
Liquid phase specific heat capacity, C_{PS} (J/kg K)	678
Temperature coefficient of surface tension, dγ /dT (N/mK)	−0.00028
Thermal expansion coefficient, β (K^{-1})	1.1×10^{-5}[24]
Magnetic permeability of vacuum, μ_0 (N/A^2)	1.26×10^{-6}[25]
Melting heat, L (J/kg)	3.57×10^5
Surface tension, σ (N/m)	1.65

B. *Simulation Procedure*

The simulation was carried out for mechanism study. The physical properties are listed in Table II. Notice that titanium alloy is paramagnetic so that its magnetic permeability μ_m will be substituted by μ_0 in this article. Other assumptions were as follows: The liquid in molten pool is a viscous, incompressible, laminar fluid; density variations follow Boussinesq approximation; and the physics of material are independent of temperature except for surface tension coefficient.

Driving forces such as surface tension, electromagnetic force (Eq. [1]), and buoyancy were known as the source term by the momentum equation of x/y direction. The model follows the mass conservation equation, momentum conservation equation of x/y direction, and the energy conservation equation.

$$\begin{cases} (J \times B)_x = \frac{-\mu_0 I^2}{4\pi^2 R_{arc}^2 r} \exp\left(\frac{-r^2}{2R_{arc}^2}\right)\left[1 - \exp\left(\left(\frac{-r^2}{2R_{arc}^2}\right)\right)\right]\left(1 - \frac{x}{h}\right) \\ (J \times B)_y = \frac{-\mu_0 I^2}{4\pi^2 h r^2}\left[1 - \exp\left(\left(\frac{-r^2}{2R_{arc}^2}\right)\right)\right]^2\left(1 - \frac{y}{h}\right), \end{cases} \quad [1]$$

where R_{arc} is the root radius of arc plasma, h is the arc length, x is the x coordinate, and y is the y coordinate.

III. RESULTS AND DISCUSSION

A. *The Arc Force and Mathematical Model*

The arc forces with different parameters are illustrated in Figure 2. The average measured results were displayed with error bars that were obtained from three replicate tests at every parameter group.

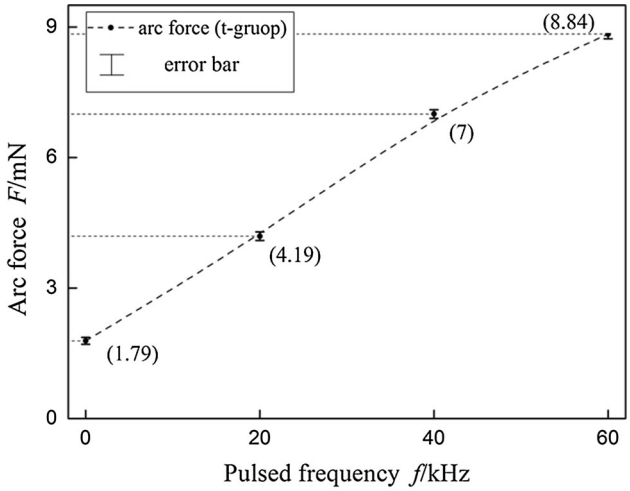

Fig. 2—The arc force with welding process.

The same changing trend can be found in t groups. The trend increased with the pulsed frequency and the maximum value was in 60 kHz. Notice that the measured value was the average arc force with one certain parameter. With the traditional point of view, the arc force distributed with Gauss, double-sided exponential distribution, or other curve models. The function of exponential distribution is represented in Eq. [2]. The coefficient a, b determined the attenuation of the force functions and the distribution characteristics. The exponent model of the arc pressure P was improved with Gaussian function in Eq. [3] It was maximum at the axis and quickly attenuated to the edge. By contrast, the parabola model was also represented in Eq. [4]. Similarly, the maximum can be found at the axis of the arc.

However, there would be slow attenuation from the center to the edge. Figure 3 illustrates the various curves with the exponent and parabola model.

$$F = F_{\max} \cdot \exp\left\{-a \cdot \left(\frac{x-b}{R_{\text{arc}}}\right)^2\right\} \quad [2]$$

where F is the arc force, $F_{\max}$ is the maximum arc force at the axis of the arc, x is the x coordinate, a is the attenuation coefficient, and b is the attenuation coefficient.

$$P = F_{\max} \cdot \exp\left\{-3 \cdot \left(\frac{x}{R_{\text{arc}}}\right)^2\right\} \Big/ \pi R_{\text{arc}}^2 \quad [3]$$

$$P = \text{sqrt}\left(-F_{\max}^2 \cdot \left(1 - e^{-2a}\right) \cdot \left(x - R_{\text{arc}}/\left(1 - e^{-2a}\right)/\pi^2 R_{\text{arc}}^5\right) \quad (0 \le x \le R_{\text{arc}}) \right. \quad [4]$$

In this study, the $F_{\max}$ was estimated to be twice than the average measured value as assumption. Different distributions can be compared to check the arc force attenuated status. Notice that the scale of x should be in $[0,R]$, which can guarantee that the equation of parabola model is valid. The area of $[0,R]$ also belongs to the correct scope with the experimental results.

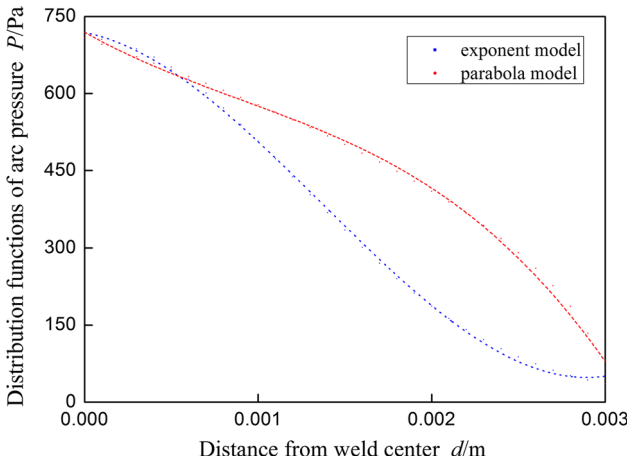

Fig. 3—Various curves with exponent and parabola models.

B. *Simulation Results*

A two-dimensional model with surface depression was produced for transient status under the effect of arc force. The VOF method with two phases was carried out. The calculation scale was 30 × 2.5 mm^2 with 25,000 cells, 50,550 faces, and 25,551 nodes.

The boundary conditions are described as follows: the top boundary is the pressure inlet (the arc force/pressure), at the axis boundary, the heat flux equals zero; at the edge and bottom boundary is a constant temperature of 300 K (27 °C).

The region patched in y = 0.002 m including 20,000 cells was set as molten metal and the space in (0.0002, 0.00025 m) was set as argon. The model and region are illustrated in Figure 4. The initialization was produced with pressure and temperature in the top boundary. The gas region above the interface was argon with a high temperature. It stands for the arc plasma during welding with pressure and temperature. The liquid region below the interface was melting metal. The arc pressure can cause an impulse on the surface of the molten pool that would create surface deformation. The surface depression will be studied with the effect of the arc force.

The arc pressure for simulation is shown in Table III. Different maximum arc forces and root radiuses were

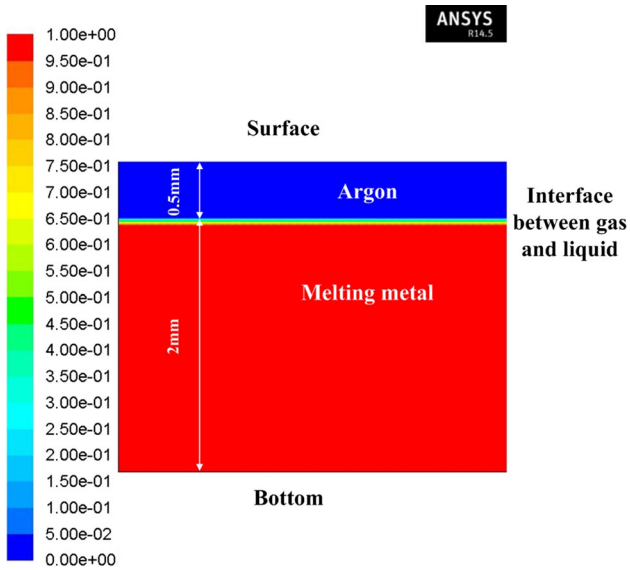

Fig. 4—Tw-dimensional model for simulation with VOF.

Table III. The Mathematical Model for Arc Pressure

No.	Exponent	Parabola ($0 \le x \le R_{\text{arc}}$)
t-1	$0.0036 \cdot \exp\left\{-3 \cdot \left(\frac{x}{R_{f=0}}\right)^2\right\}/\pi R_{f=0}^2$	$\text{sqrt}\left(-1.293 \cdot 10^{-5} \cdot \left(x - R_{f=0}/\left(9.845 \cdot R_{f=0}^5\right)\right)\right.$
t-2	$0.0084 \cdot \exp\left\{-3 \cdot \left(\frac{x}{R_{f=20}}\right)^2\right\}/\pi R_{f=20}^2$	$\text{sqrt}\left(-7.039 \cdot 10^{-5} \cdot \left(x - R_{f=20}/\left(9.845 \cdot R_{f=20}^5\right)\right)\right.$
t-3	$0.014 \cdot \exp\left\{-3 \cdot \left(\frac{x}{R_{f=40}}\right)^2\right\}/\pi R_{f=40}^2$	$\text{sqrt}\left(-1.96 \cdot 10^{-4} \cdot \left(x - R_{f=40}/\left(9.845 \cdot R_{f=40}^5\right)\right)\right.$
t-4	$0.018 \cdot \exp\left\{-3 \cdot \left(\frac{x}{R_{f=80}}\right)^2\right\}/\pi R_{f=80}^2$	$\text{sqrt}\left(-3.232 \cdot 10^{-4} \cdot \left(x - R_{f=80}/\left(9.845 \cdot R_{f=80}^5\right)\right)\right.$

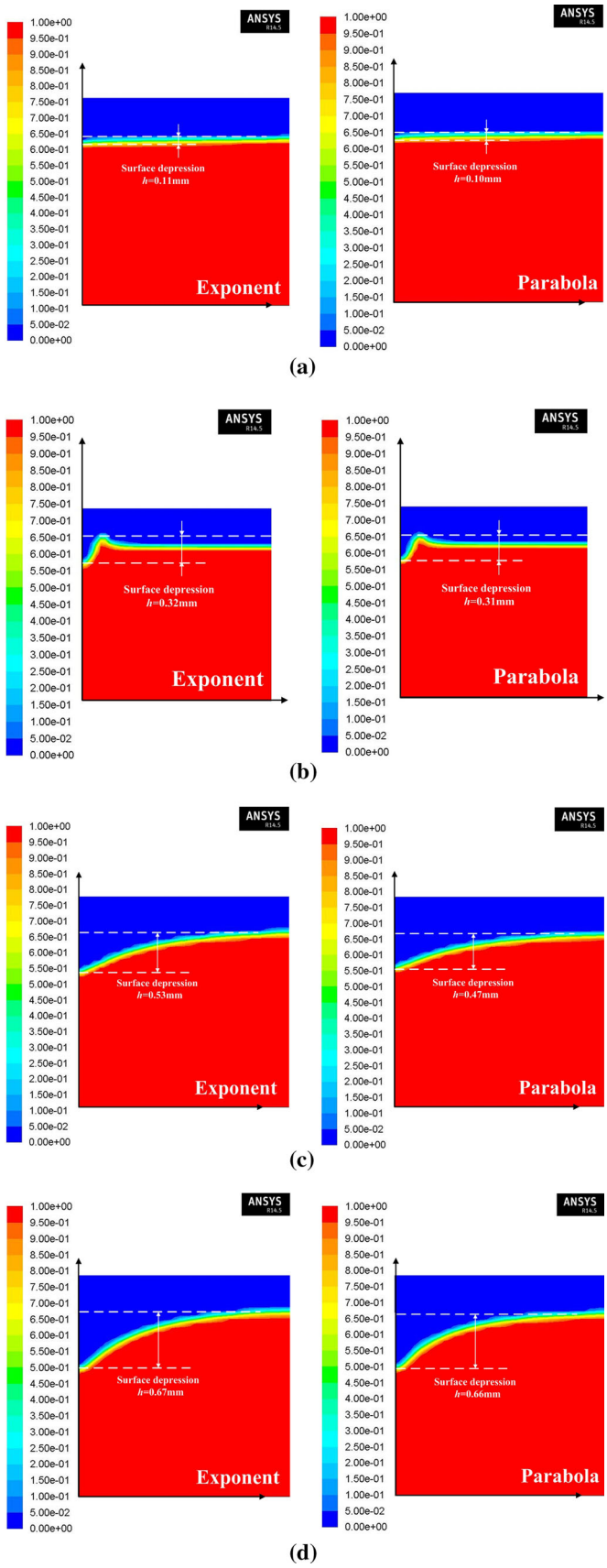

Fig. 5—Surface depression with different arc forces.

Table IV. Comparison of Calculated and Simulated Results

No.	Calculated (mm)	Simulated		
		Exponent (mm)	Parabola (mm)	Average Error (pct)
t-1	0.12	0.11	0.10	12.5
t-2	0.31	0.32	0.31	1.6
t-3	0.53	0.53	0.47	5.6
t-4	0.67	0.67	0.66	0.7

used to calculate the distribution. The simulated results are illustrated in Figure 5. Furthermore, the surface depression at the axis was compared with the previous work in Reference 22. All the simulated values will be obtained with 10^{-5} seconds time step size for more than 4500 steps. Figure 5(a) demonstrates that the surface depression is very limited with C-GTAW. The results with exponent and parabola model were similar. The surface depressions were 0.11 and 0.10 mm, respectively. As described in Section I, the effect of arc force on surface depression can be found with more than 200 A.[26] The experimental design with 80 A was less than 200 A absolutely. Thus, significant deformation with C-GTAW was not hypothesized. Furthermore, the error with small arc force will be 8 to 16 pct because of the little surface depression.

The arc force had an effect on surface fluid at 20 kHz, and the depressions were 0.32 and 0.31 mm with exponent and parabola models, which was matched well with the calculated results. With 40 kHz, the surface depressions increased to be 0.53 and 0.47 mm, which was caused by large impulses of arc plasma or arc force. The pressure pushed the fluid from the molten pool to the edge of welds. Almost no surface fluctuation was captured. Although the pulsed frequency equals 60 kHz, significant surface depressions can be found with both exponent and parabola distributions. They reached more than 0.65 mm, which led to a huge deformation in the molten pool. Noticed that the arc force had been 8.84 mN with the titanium alloy, and an obvious arc fluid appeared near the axis of depression. However, no arc-shaped depression can be found with the simulated results. It could be because the calculated process (arc-shaped assumption in Reference 22) ignored the resistance of fluid. In this study, the VOF model with fluid simulation can support resistance during arc welding. Thus, it is also believed that no arc-shaped surface depression will happen during the actual welding process. Even so, the arc-shaped assumption is also a good method for basic research with low welding current.

In addition, the results were compared with the previous data. The surface depressions were 0.12, 0.31, 0.53, and 0.67 mm, respectively (Reference 22). The VOF model simulated the surface depression with various parameters that calculated the heights of the depression. With the pulsed arc welding process, although different distribution mathematical model determined different results, that still meant less error (<13 pct) between calculated and simulated data as shown in Table IV.

Above all, the simulation indicated that the results with exponent model were more accurate than parabola distribution. The error was less than 3.3 pct with pulsed arc welding. Thus, it can be concluded that the distribution of the arc force had quick attenuation to the edge of the arc plasma. The significant arc constriction with pulsed arc welding may contribute most to these results.

IV. CONCLUSIONS

The impact of arc force was recognized as the reason for the surface depression during arc welding. This article discussed the mathematical distribution of arc force with exponent and parabola models. The comparison was mentioned with the simulation results. The results indicated that the average arc force increased with pulsed frequencies during UHFP-GTAW. The surface depression was estimated to be caused by the arc force. The geometry of the surface depression was discussed with liquid metal. The curve profiles were studied with the arc force distributions, and the results showed that the exponent model was more accurate to the as-weld condition. The error between the calculated and simulated results was less than 3.3 pct with UHFP-GTAW. Thus, the study concluded that the distribution of the arc force had quick attenuation to the edge of the arc plasma.

ACKNOWLEDGMENTS

This work was supported by the National Natural Science Foundation of China under Grant No. 51405007 and Fundamental Research Funds for the Central Universities of China. All support from Beijing University of Aeronautics and Astronautics is highly appreciated.

REFERENCES

1. C.S. Wu, J. Chen, and Y.M. Zhang: *Comput. Mater. Sci.*, 2007, vol. 39, pp. 635–42.
2. J. Hu, H. Guo, and H.L. Tsai: *Int. J. Heat Mass Trans.*, 2008, vol. 5, pp. 2537–52.

3. F. Lu, S. Yao, S. Lou, and Y. Li: *Comput. Mater. Sci.*, 2004, vol. 29, pp. 371–78.
4. M.L. Lin and T.W. Eagar: *Weld. J.*, 1985, vol. 64, pp. 162s–69s.
5. S. Kou and Y.H. Wang: *Metall. Trans. A*, 1986, vol. 17A, pp. 2271–77.
6. M.C. Tsai and S. Kou: *Weld. J.*, 1990, vol. 69, pp. 241s–46s.
7. C. Jia, K. Xiao, and X. Yin: *J. Xi'An Jiaotong Univ.*, 1994, vol. 28, pp. 23–28.
8. G.E. Cook, H. El-deam, and E.H. Eassa: *IEEE Trans. Indust. Appl.*, 1985, vol. 21, pp. 1294–99.
9. R.T.C. Choo and J. Szekely: *Weld. J.*, 1991, vol. 70, pp. 223s–33s.
10. S.I. Rokhlin and A.C. Guu: *Weld. J.*, 1993, vol. 72, pp. 381s–90s.
11. P.K. Ghosh, L. Dorn, M. Hübner, and V.K. Goyal: *J. Mater. Process. Tech.*, 2007, vol. 209, pp. 163–75.
12. O. Jin, A. Yoshisa, N. Masayasu, K. Mitsuo, A. Onuma, and T. Funamoto: *Japan. J. Appl. Phys.*, 2002, vol. 41, pp. 5821–26.
13. B.J. Qi, M.X. Yang, B.Q. Cong, and F.J. Liu: *Int. J. Adv. Manuf. Tech.*, 2013, vol. 66, pp. 1545–53.
14. Q. Yunlian, J. Deng, Q. Hong, and L. Zeng: *Mater. Sci. Eng. A*, 2000, vol. 280, pp. 177–81.
15. W.A. Baeslack, III and C.M. Banas: *Weld. J.*, 1981, vol. 60, pp. 121s–30s.
16. H.J. Aval, A. Farzadi, S. Serajzadeh, and A.H. Kokabi: *Int. J. Adv. Manuf. Technol.*, 2009, vol. 42, pp. 1043–51.
17. M. Balasubramanian, V. Jayabalan, and V. Balasubramanian: *Acta Metall. Sinica*, 2010, vol. 23, pp. 312–20.
18. M. Yang, B. Qi, B. Cong, and F. Liu: *Int. J. Adv. Manuf. Tech.*, 2013, vol. 68, pp. 19–31.
19. Z.X. Ge, H.M. Chen, and Y. Ge: *Hot Working Tech.*, 2004, vol. 7, pp. 47–48.
20. V. Balasubramanian, V. Jayabalan, and M. Balasubramanian: *Mater. Design*, 2008, vol. 29, pp. 1459–66.
21. M. Balasubramanian, V. Jayabalan, and V. Balasubramanian: *Mater. Lett.*, 2008, vol. 62, pp. 1102–06.
22. M. Yang, Z. Yang, B. Cong, and B. Qi: *Weld. J.*, 2014, vol. 93, pp. 312s–19s.
23. R. Boyer, G. Welsch, and E.W. Collings: *Materials Properties Handbook: Titanium Alloys*, ASM International, Materials Park, OH, 1994.
24. S. Mishra and T. DebRoy: *Acta Mater.*, 2004, vol. 52, pp. 1183–92.
25. G.M. Oreper and J. Szekely: *Metall. Trans. A*, 1987, vol. 18A, pp. 1325–32.
26. S.H. Ko, S.K. Choi, and C.D. Yoo: *Weld. J.*, 2001, vol. 80, pp. 39s–45s.